様　式　Ｃ－１９、Ｆ－１９、Ｚ－１９　（共通）

科学研究費助成事業　　研究成果報告書

平成　２７　年　　６　月　２２　日現在

機関番号：　２２６０４
研究種目：　若手研究(B)
研究期間：　2013～2014
課題番号：　２５８７０５９４

研究課題名（和文）Microstructure Refinement and Control of Metal Tubes with a Novel Rotating Bending Process

研究課題名（英文）Microstructure Refinement and Control of Metal Tubes with a Novel Rotating Bending Process

研究代表者

張　自成（Zhang, Zicheng）

首都大学東京・理工学研究科・客員研究員

研究者番号：１０６４２６７１

交付決定額（研究期間全体）：（直接経費）　　3,400,000円

研究成果の概要（和文）：本研究では，金属管の繰返し回転曲げ（CRB）による結晶粒の微細化および制御法の提案を行った．加熱温度，曲げ半径，累積塑性ひずみ等が加工後の結晶組織の及ぼす影響を調査した．また加工によって累積する塑性ひずみを予測するモデルを提案し，その妥当性を示すことができた．その結果，結晶組織は微細化することが明らかになった．また各種条件の設定により，所望の結晶粒径と機械的特性を得られることがわかり，本プロセスの有効性を示すことができた．

研究成果の概要（英文）：To refine and control the microstructure of metal tubes the cyclic rotating bending (CRB) process was proposed. The effects of the deformation temperature, bending radius, cumulative strain, and internal stress and strain distribution influence on the grain size were investigated. The predictive models to characterize the deformation behavior of metal tubes in rotating bending process was proposed. The microstructure of all of the metal tubes were refined by the CRB process. It was also found that the rotating bending process showed different refinement effects on different kind of metal tubes. As a result, to obtain the expected grain size and mechanical properties of the tube the suitable parameters for different kind of metal tubes should be optimized according to the characteristics of the deformation behavior of the metal tubes during the CRB process.

研究分野：　Engineering Plasticity

キーワード：　金属管　強加工　繰返し曲げ加工　結晶粒微細化　累積塑性ひずみ

１．研究開始当初の背景

The automotive lightweighting technologies promoted the popularization and application of metal tubes in automobile industry since using the hollow structure produced with metal tubes instead of the solid ones can significantly reduce the automobile weight. According to the manufacturing method, the metal tubes can be divided into seamless tubes, such as hot-rolled tube, cold-rolled tube, cold-drown tube, extruded tube, jacking tube, etc. and welded tubes, such as arc welded tube, resistance welded tube, gas welded tube, furnace welded tubes. The metal tubes produced with these methods are often accompanied by grain coarsening, uneven microstructure and ductility deterioration. It is very often that the uniform refined microstructure and good ductility are both required in the application field of metal tubes. To obtain a uniform fine microstructure the heat treatment method is usually conducted. However, the heat treatment process often leads to the grain coarsening and deterioration of mechanical properties. To obtain the desired microstructure and improve the mechanical properties of metal tubes a rotating bending process was newly proposed, as shown in **Fig. 1**. The preliminary experimental results show that this method can be used to refine and control the microstructure of metal tubes. However, the further investigation is urgently needed to be performed to attain a better insight into the deformation behavior of metal tubes and to clarify how the parameters of rotating bending process such as deformation temperature, bending radius, cumulative strain, and internal stress and strain distribution influence on the controlling and refining of metal tubes microstructure. How to predict the evolution of microstructure during the deformation process for metal materials with numerical simulation has been attracting increasing attentions in the last several decades. Accurate prediction of microstructure evolution in forming process with simulation can give a good advising to the real experiment and reduce the number of trials as well as cost in industry.

The existent reports in microstructure simulation mainly focused on rolling, casting and hot forging processes. During these forming processes the status of stress and strain of deforming material is relative simple. The simulation of microstructure evaluation under the complex deformation conditions is a new trend which has been attracting more and more attentions in the worldwide. However, the reports on the microstructure simulation of material under complex deformation conditions are rare seen. In the proposed research, the metal tubes are simultaneously subjected to the tensile and compress plastic strain in rotating bending process. Therefore, a new model for microstructure evolution for metal tubes under tensile and compress plastic strain should be proposed.

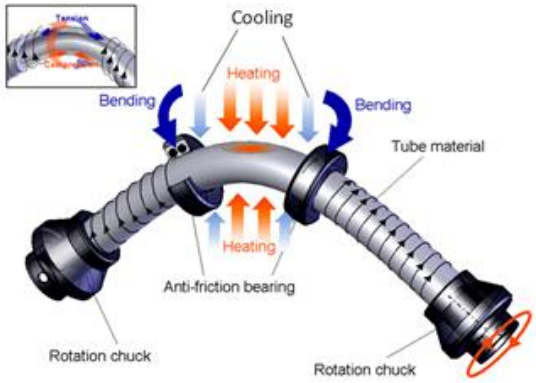

Fig. 1 Schematic drawing of newly proposed rotating bending process

２．研究の目的

The main purpose of the current research are summarized as follows.

1) To develop an experimental method for grain refining and microstructure control of metal tubes.

2) To clarify how the factors such as deformation temperature, bending radius, cumulative strain, and internal stress and strain distribution influence on the grain size, crystal orientation and surface characteristics of metal tubes.

3) To develop predictive models (FEM) to characterize the deformation behavior as well as microstructure evolution of bending part of metal tubes in rotating bending process at different forming conditions.

３．研究の方法

(1) Experiments

The dimension of the magnesium alloy tube is Φ12.8×0.8(thickness)×200(length) mm. The bending angle is about 150° obtained by calculation based on the geometric relationships and mechanical relationships. To investigate the effect of the rotating bending process on microstructure of magnesium alloy tube at different temperature, the rotating bending processes were carried out at 150, 200, 250, 300 and 350°C with a rotation speed of 20r/min for 10min. The heat treatments were also carried out at 150, 200, 250, 300 and 350°C for 10min to obtain the microstructure and mechanical properties of the tubes without rotating bending deformation. To clarify the effect of accumulated plastic strain on the microstructure and mechanical properties of AZ31 magnesium alloy tube, the rotating bending process was carried out with a rotation speed of 20r/min for 2, 6 and 10min at temperature conditions of 150, 200 and 250°C. The tubes were immediately quenched

with water after rotating bending process and heat treatment process.

(2) Theoretical calculation

Fig. 2 shows the schematic diagram of newly proposed rotating bending process. Here the method to confirm the neutral layer of the bent tube proposed by Tang et al. was used to determine the neutral layer of bent metal tube with rotating bending process.

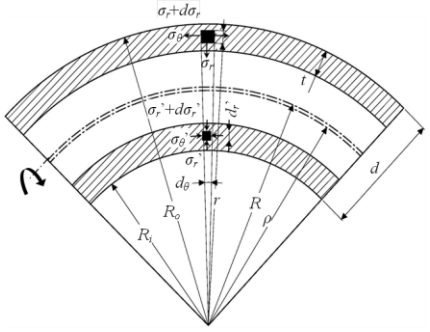

Fig. 2 Stress state model of metal tube in bending process

Assumptions:

i) The cross-section of tube remained unchanged before and after bending process; ii) The bending process satisfies constant volume principle of plastic deformation; iii) The equivalent stress and strain satisfy the equation $\bar{\sigma} = K\bar{\varepsilon}^n$, where K is the strain hardening coefficient of metal tube, n is the material hardening exponent.

Fig. 2 shows the stress state model of metal tube in horizontal section in bending process. d, t and t_0 are the outside diameter, instantaneous thickness and initial thickness of metal tube, respectively. r is the bend radius of selected point in the tube. ρ is the curvature of the bending neutral layer. R_i and R_o are the radius of concave and convex sides of bent tube, respectively. σ_θ is the tangential stress. σ_r is the radial stress. In addition there is also circumferential stress, σ_φ, in the cross-section of bent tube.

Due to the assumption i), it can be known that circumferential strain ε_φ=0. The bent tube is in the plane strain state with the tangential strain, ε_θ, and radial strain, ε_r, where

$$\varepsilon_\theta = \ln(r/\rho),\ \ \varepsilon_r = \ln(t/t_0) \qquad (1)$$

According to the assumption ii),

$$\varepsilon_\theta + \varepsilon_r + \varepsilon_\varphi = 0. \qquad (2)$$

Because ε_φ=0, $\varepsilon_\theta = -\varepsilon_r$, that is

$$\ln(r/\rho) = -\ln(t/t_0) \qquad (3)$$

Substitute ε_φ=0 to the Hencky equation,

$$\sigma_\varphi = (\sigma_\theta + \sigma_r)/2. \qquad (4)$$

Substitute Eq. (5) and ε_φ=0 to the Mises yield criterion,

$$\bar{\sigma} = \sqrt{(1/2)\left[(\sigma_\theta-\sigma_r)^2+(\sigma_r-\sigma_\varphi)^2+(\sigma_\varphi-\sigma_\theta)^2\right]} = (\sqrt{3}/2)|\sigma_\theta-\sigma_r| \qquad (5)$$

$$\bar{\varepsilon} = \sqrt{(2/3)(\varepsilon_\theta^{\ 2}+\varepsilon_r^{\ 2}+\varepsilon_\varphi^{\ 2})} = (2/\sqrt{3})|\varepsilon_\theta|. \qquad (6)$$

Substitute Eq. (1), (5) and (6) to $\bar{\sigma} = K\bar{\varepsilon}^n$,

$$\sigma_\theta - \sigma_r = \pm(2/\sqrt{3})^{1+n} K(\pm\ln(r/\rho)) \qquad . \qquad (7)$$

For the micro unit in Fig. 1, according to the equilibrium of forces in the radial direction, the following equation can be obtained (omitting the tiny quantities of high order

$$d\sigma_r/dr = (\sigma_\theta - \sigma_r)/r. \qquad (8)$$

The radial stress σ_r can be obtained by integration.

$$\sigma_r = (2/\sqrt{3})^{1+n}(K/(1+n))(\pm\ln(r/\rho)) + C, \quad (9)$$

where C is the integration constant.

In Fig. 1, in the surface of concave ($r = R_o$) and convex sides ($r = R_i$) of bent tube, the radial stress σ_r=0. In the neutral layer ($r = \rho$), σ_r is a continuous variable. So the integration constants can be confirmed when $r > \rho$ and $r < \rho$.

$$C_1 = -(2/\sqrt{3})^{1+n}(K/(1+n))(\ln(R_w/\rho))^{1+n}, \quad (10)$$

$$C_2 = -(2/\sqrt{3})^{1+n}(K/(1+n))(-\ln(R_w/\rho))^{1+n}, \quad (11)$$

When $r=\rho$ it can be known that $C_1 = C_2$.

Then the curvature of the bending neutral layer was obtained.

$$\rho = \sqrt{R_i \cdot R_o}. \qquad (12)$$

Fig. 3 shows the schematic diagram of the cross-section of bent tube with considering the offset of neutral layer and the stress status distribution in the bent tube cross-section. To determine the equivalent strain of the tube during the bending process, the cross-section of bent tube can be divided into plastic zone and elastic zone, as shown in Fig. 3. Here, only the plastic deformation was considered for the purpose of simplifying the calculation.

As the tube cross-section was assumed as unchanged and according to the principle of constant volume, the

$$\varepsilon_\theta = \ln(r/\rho),\ \varepsilon_\varphi = 0,\ \varepsilon_r = \ln(t/t_0). \qquad (13)$$

$$\varepsilon_\theta + \varepsilon_r + \varepsilon_\varphi = 0. \qquad (14)$$

The equivalent strain ε_e can be expressed as

$$\varepsilon_e = \sqrt{\frac{2}{9}\left[(\varepsilon_r-\varepsilon_\varphi)^2+(\varepsilon_\varphi-\varepsilon_\theta)^2+(\varepsilon_\theta-\varepsilon_r)^2\right]} = \frac{2}{\sqrt{3}}\varepsilon_r \qquad (15)$$

The accumulated equivalent strain for one tiny unit of bent tube along the circumferential

direction $d\varepsilon_e$ was given as

$$d\varepsilon_e = \frac{2}{\sqrt{3}} d\varepsilon_r . \tag{16}$$

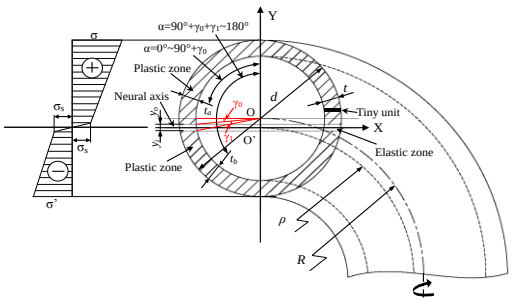

Fig. 3 Schematic diagram of the cross-section of bent tube with considering the offset of neutral layer and the stress status distribution in the bent tube cross-section

In the outside of neutral layer of bent tube, the accumulated equivalent strain $\bar{\varepsilon}_{AS}$ was obtained as

$$\bar{\varepsilon}_{AS} = 2\int d\varepsilon_e = 2\int \frac{2}{\sqrt{3}} d\varepsilon_r = \frac{4}{\sqrt{3}}\int \ln(\frac{t_a}{t})dt = \frac{4}{\sqrt{3}}\int_0^{90°+\gamma_0} \ln\left[\frac{(1-\frac{2k+\cos\alpha}{4k+3-\cos\alpha}\frac{\cos\alpha}{2k})t}{t}\right] d\alpha$$

$$= \frac{4}{\sqrt{3}}\int_0^{90°+\gamma_0} \ln\left(1-\frac{2k+\cos\alpha}{4k+3-\cos\alpha}\frac{\cos\alpha}{2k}\right) d\alpha. \tag{17}$$

In the inside of neutral layer of bent tube, the accumulated equivalent strain $\bar{\varepsilon}_{AS}'$ was obtained as

$$\bar{\varepsilon}_{AS}' = 2\int d\varepsilon_e = 2\int \frac{2}{\sqrt{3}} d\varepsilon_r = \frac{4}{\sqrt{3}}\int \ln(\frac{t_b}{t})dt = \frac{4}{\sqrt{3}}\int_{90°+\gamma_0+\gamma_1}^{180°} \ln\left[\frac{\left(1-\frac{2k+2-\cos\alpha}{4k+1-\cos\alpha}\frac{\cos\alpha}{2k}\right)t}{t}\right] d\alpha$$

$$= \frac{4}{\sqrt{3}}\int_{90°+\gamma_0+\gamma_1}^{180°} \ln\left(1-\frac{2k+2-\cos\alpha}{4k+1-\cos\alpha}\frac{\cos\alpha}{2k}\right) d\alpha. \tag{18}$$

The total accumulated equivalent strain $\bar{\varepsilon}_{TAS}$ for one tiny unit of bent tube in one revolution along the circumferential direction was obtained as

$$\bar{\varepsilon}_{TAS} = \left|\bar{\varepsilon}_{AS}\right| + \left|\bar{\varepsilon}_{AS}'\right| = \left|\frac{4}{\sqrt{3}}\int_0^{90°+\gamma_0} \ln\left(1-\frac{2k+\cos\alpha}{4k+3-\cos\alpha}\frac{\cos\alpha}{2k}\right) d\alpha\right| + \left|\frac{4}{\sqrt{3}}\int_{90°+\gamma_0+\gamma_1}^{180°} \ln\left(1-\frac{2k+2-\cos\alpha}{4k+1-\cos\alpha}\frac{\cos\alpha}{2k}\right) d\alpha\right|$$

$$= \frac{4}{\sqrt{3}}\left[\left|\int_0^{90°+\gamma_0} \ln\left(1-\frac{2k+\cos\alpha}{4k+3-\cos\alpha}\frac{\cos\alpha}{2k}\right) d\alpha\right| + \left|\int_{90°+\gamma_0+\gamma_1}^{180°} \ln\left(1-\frac{2k+2-\cos\alpha}{4k+1-\cos\alpha}\frac{\cos\alpha}{2k}\right) d\alpha\right|\right]. \tag{19}$$

The accumulated equivalent strain $\bar{\varepsilon}_{Total}$ for the bent tube with a rotation speed of v r/min for T min can be expressed as

$$\bar{\varepsilon}_{Total} = v \cdot T \cdot \bar{\varepsilon}_{TAS} . \tag{20}$$

(3) FEM model

Fig. 4 shows the mashed tube and bush. The solid element was used. The total number of the element for the tube is 5616 for tube. The total number of element is 4000 for bush. The bending angle is set as 173°. The rotation speed is 20rpm. The deformation temperature is 200°C.

Fig. 4 Mesh models of the tube and bush

4．研究成果

(1) Experimental results

Fig. 5 shows the optical microstructure in the longitudinal section of selected samples with temperature conditions of 150, 200, 250 and 350°C. It can be seen that the grain number increased significantly in the relative area after rotating bending process. There were new grains formed in all samples. It means that the recrystallization occurred in high strain rate even in a relative low deformation temperature of 150°C, which made a significant contribution to the refining of grains. The grain boundaries became coarse and the grain shapes changed into approximate square from nearly circular when the deformation temperature increased to 250 and 350°C, as shown in Fig. 5(g) and (f). In the current study, the tensile and compressive deformations were alternately subjected to the bending part of tube. Under the act of strong plastic deformation the continuous dynamic recrystallization (CDRX) was observed for all the pre-set temperature conditions even at a relative low temperature of 150°C. After plastic deformation at low temperature region (150 and 200°C), the dense dislocation piled up in the interior of grains accompanied by the forming of a large number of twins. During the deforming process the lamellar twins grew up and the microcrystal formed between the lamellar twins due to the twin dynamic recrystallization (TDRX). The further deformation leads to the grain boundary large-scale migration. This process results in the recrystallized grains growing up and the increase of its volume fraction. When the plastic deformation happened at the medium temperature region (250 and 300°C), the basal and non-basal planes slipping concurred simultaneously accompanied by the cross slip. The recrystallization type are CDRX indicated by Barnett. When the temperature is high than 350°C, the initial strong deformation leads to the original twin grain boundary migration. At the same time, the CDRX occurred along the original grain boundaries and twin boundaries. The further deformation actuated the recurrent CDRX. The average grain size was

reduced due to the newly generated fine grains. The similar results were also reported by Jiang et al. by carrying out the tensile tests at various temperatures using as-extruded AZ31 magnesium alloy.

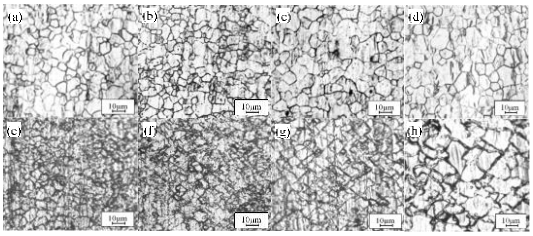

Fig. 5 Microstructure in longitudinal section of selected samples ((a) and (e): 150°C; (b) and (f): 200°C; (c) and (g): 250°C, (d) and (h): 350°C), ((a), (b), (c) and (d): without bending; (e), (f), (g)and (h): with bending)).

The room temperature tensile properties of the selected samples at different temperatures with a rotation speed of 20r/min for 10min are shown in **Fig. 6**. The rotating bending process carried out at room temperature (RT) resulted in the increase of strength. But the ductility deteriorated comparing to the as-extruded tube. When the rotating bending temperature was 150°C, the strength decreased but the ductility increased after rotating bending process. But the ductility of both samples with and without rotating bending deformation became worse than the as-extruded tube. With the rotating bending temperature increased to 200°C, the strength as well as ductility was improved for both samples with and without bending. The sample with rotating bending deformation shows better mechanical properties than the one without rotating bending deformation. However, when the rotating bending temperature was 250°C, the mechanical properties became worse for both samples than the as-extruded tube. And the mechanical properties were degenerated by the rotating bending process.

When the rotation temperature is low, the grain growing rate is slow. In addition, the strong deformation promoted the recrystallization process in the microstructure. The grains were significantly refined. As the grain size is small, the strong deformation had little effect of on the grain shape as well as grain boundaries. Therefore, the ductility of the sample increased after rotating bending process as its refined grains. However, when the deformation temperature was higher than 250°C, the grain growing rate was high. As though the deformation process was accompanied by the recrystallization process, the grain size also significantly increased comparing to the as-extruded tube, as shown in Fig. 2. This result is agreed with the one reported by Yang, et al.. For the rotating bending process, in the compression time the coarse grains collided with each other, but in the tension time the grains were under tensile stress state and they tried to separate to each other, which resulted in the grain shape change and the coarsening of grain boundaries. Thus, the mechanical properties did not become better even the grains were refined when the deformation temperature was 250°C.

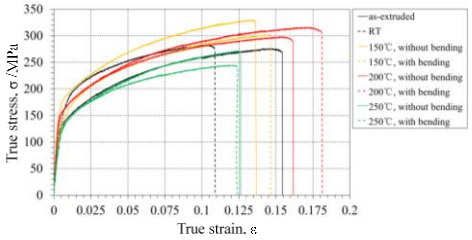

Fig. 6 True stress vs. true strain curves of selected samples at different temperatures with a rotation speed of 20r/min for 10min

(2) Theoretical calculation

To verify the validity of the proposed formula for determining the accumulated equivalent plastic strain of bending part in metal tube rotating bending process, the rotating bending experiments with different bending radii were carried out at room temperature with the Aluminum alloy tubes with the dimension of 10(diameter)×2(thickness)×200mm. The rotating bending process was carried out with a rotation speed is 20r/min for 5min. The grid method was used in the experiment to determine the accumulated equivalent strain of tube bending part. The calculation results of accumulated equivalent plastic strain with the proposed formulas and the ones obtained with experiments for one round are summarized in **Table 1**. It can be seen that the calculation results have a good agree with the ones obtained in the experiments.

Table 1 Calculation results of accumulated equivalent plastic strain with proposed formulas and obtained in experiments for one round

Bending angle, °	Calculation results	Experimental results	Error, %
173.0	0.532	0.559	4.83
165.8	0.712	0.742	4.04
158.7	0.839	0.864	2.89

(3) FEM results

Fig. 7 shows the temperature distribution map of tube during preheating and CRB process. The heating time is 10s. The time for bending is 5s. The time for rotating bending process is 300s. It can be seen that the temperature decreased with form central point to the end of the tube. The central point showed the highest temperature of

200 °C. The temperatures of the tube ends are near to the room temperature.

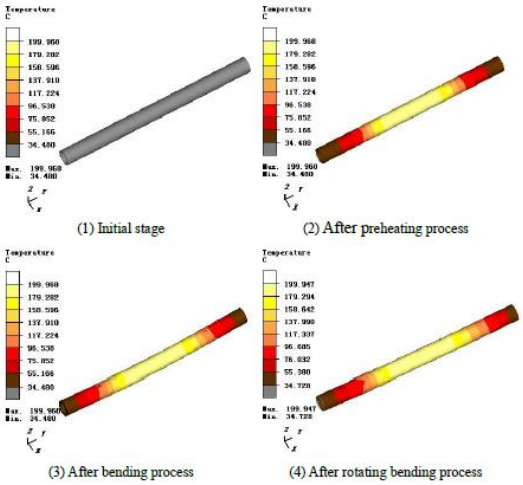

Fig.7 Temperature distribution map of tube during CRB process (Heating time is 10s. The time for bending is 5s. The time for rotating bending process is 300s.)

Fig. 8 shows the effective plastic strain values at selected points in surface of tube during one cycle of rotating bending process. It can be seen that the effective plastic strain values of all the points increased with the increase of rotation number from zero to 1 except point 9 which located in the end of tube. It also can be known that the point 3 show a higher value than other points include point 5 which located in the center of tube.

Fig. 9 presents the comparison between the selected points in the outside and inside surface in tube center. It can be seen that for one circle of rotating deformation the points in the outside surface of tube shows a higher values of effective plastic strains than that of the points in the inside surface of the tube. The growth movement of the values for the points in the inside surface or in the outside surface are approximate.

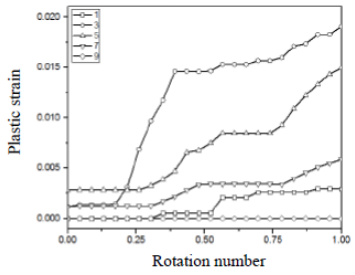

Fig.8 Effective plastic strain values at selected points during one cycle of rotating bending

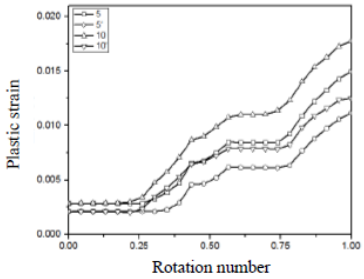

Fig.9 Effective plastic strain values at selected points on inner and outer surface

５．主な発表論文等
（研究代表者、研究分担者及び連携研究者には下線）

〔雑誌論文〕（計 1 件）

① Zhang, Z.C., Manabe, K., Furushima, T., Tada, K., Formulation of Equivalent Plastic Strain Accumulated in Rotating Bending Process of Metal Tubes for Severe Plastic Deformation, Advanced Materials Research, 887-888 (2014) 907-911, http://www.scientific.net/AMR.887-888.907（査読有）

〔学会発表〕（計 2 件）

① 真鍋健一，張自成，古島剛，高橋健太，回転繰返し強加工による銅管の結晶粒微細化，日本銅学会第 54 回講演大会，2014 年 11 月 8 日～9 日，横浜国立大学（神奈川県横浜市）

② Zhang, Z.C., Formulation of Equivalent Plastic Strain Accumulated in Rotating Bending Process of Metal Tubes for Severe Plastic Deformation, 4th International Conference on Advances in Materials and Manufacturing Processes (ICAMMP2013), 2013 年 12 月 19 日，Kunming, China

〔図書〕（計 0 件）

〔産業財産権〕
○出願状況（計 0 件）
○取得状況（計 0 件）

〔その他〕
ホームページ等

６．研究組織
(1)研究代表者
首都大学東京・理工学研究科・客員研究員
張　自成（ZHANG Zicheng）
研究者番号：１０６４２６７１